# $\Sigma^- p$ Elastic Scattering in the CLAS Detector: A Feasibility Study Using Monte Carlo Techniques

Aya Ghaleb
Department of Physics,
University of York

May, 2022

**Abstract**

A study of $\Sigma^- p \to \Sigma^- p$ elastic scattering using a Monte Carlo technique is presented. Simulations are performed in a ROOT computational framework to obtain reaction kinematics and simulate the CLAS detector acceptances, with the aim of assessing the feasibility of an experiment driven by the JLab accelerator. The motivation behind this study is the need to improve on the present hyperon-nucleon scattering data. Such advances will help constrain hyperon-nucleon interactions and may thereby assist in the resolution of the so-called ”hyperon puzzle” in neutron star physics. The simulations results are based on a 100 days of JLab beamtime. The $\Sigma^-$ particles are accumulated in the target from photoproduction, and the scattering of these particles is then observed. The measured $\Sigma^- p \to \Sigma^- p$ yield is $306,790$ $(\pm 0.2\%)$. This study supports the feasibility of a $\Sigma^- p$ elastic scattering experiment at JLab with a high yield for the momentum range 0.5-2.5 GeV/c, extending the dataset to higher momenta.

# 1 Introduction

Hyperons, baryons containing at least one strange quark, were first observed in 1947 during an experimental study of cosmic rays passing through a cloud chamber [1]. The first hypernucleus, meaning a nucleus that contains at least one hyperon, was subsequently discovered in 1953 [2], leading to the development of the field of hypernuclear physics. Today, hypernuclear physics is an active area of research lying at the intersection of nuclear and elementary particle physics, some of the findings of which have important implications for astrophysics [3].

In 1960, the first theoretical indications of the presence of stable hyperons (such as $\Lambda$ and $\Sigma$) in the core of neutron stars were reported [4]. In the neutron star inner core, the density is at least twice that of an atomic nucleus $n_0$ [5]. Neutrons, the most abundant nuclei in neutron stars, have a chemical potential which increases rapidly with density, hence in the very dense core the chemical potential is large enough that some of the energetic neutrons might decay into hyperons via the weak interaction [6]. Hence a neutron star can be thought of as a "giant hypernucleus".

The onset of hyperon formation occurs at about $2-3n_0$ [5]. The first hyperons to appear are believed to be $\Lambda$, made of an up, a down and a strange quark, and $\Sigma^-$, made of two down quarks and a strange quark. Typical processes that lead to their formations are [4]

$$p + e^- \rightarrow \Lambda + \nu_e \ ,$$
$$n + e^- \rightarrow \Sigma^- + \nu_e$$

The expected presence of such particles in the inner core of neutron stars sets constraints on their properties. One way in which this could be apparent is through their effect on the equation of state (EOS). The presence of hyperons provides additional degrees of freedom beyond those available in regular nuclear matter (i.e. protons and neutrons). This affects the neutron star EOS by making it "softer" with respect to the pure nucleonic case [6].

The terms "soft" and "stiff" can be used to describe the compressibility of nuclear matter. A simplified description of the equation of state is that it gives the variation of pressure with density. A stiff EOS is one where the increase in pressure with density is relatively large. For a neutron star, this means more support against gravitational collapse. A soft EOS, on the other hand, produces a smaller increase in pressure for a given increase in density, making it easier to compress. This pressure-density relationship [7], in turn, affects the masses and radii of neutron stars. A softening of the equation of state gives a smaller radius for the same mass and, as a consequence, reduces the maximum mass allowed for a neutron star [8].

While previously the prediction for the maximum neutron star mass ranged from $1.8$ to $2.4M_\odot$, the presence of hyperons was suggested to reduce the maximum permissible mass of neutron stars to less than $1.5M_\odot$ [3]. This is illustrated in Figure 1 taken from Ref [9].

The reported observations of neutron stars with measured masses of $M = 1.97 \pm 0.04M_\odot$ [10] and $M = 2.01 \pm 0.04M_\odot$ [11] in 2010 and 2013 are also marked in Figure 1. These measurements rule out the currently proposed equations of state that include

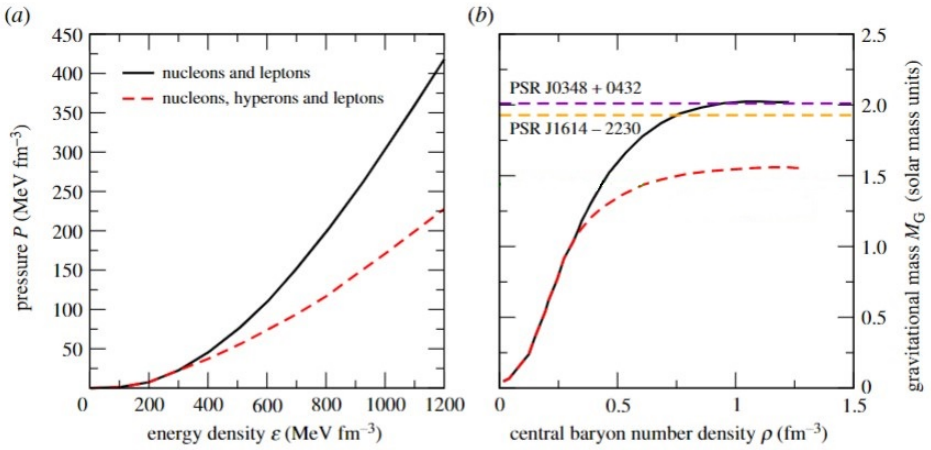


Figure 1: Illustration of the effect of the presence of hyperons on the EOS (panel (a)) and mass of a neutron star (panel (b)). A generic model with (red dashed line) and without (black solid line) hyperons is considered [9]. The horizontal lines shows the measured masses of PSR J1614-2230 [10] and PSR J0348+0432 [11] neutron stars.

hyperons. This conflict between astronomical observations and theoretical predictions is known as the ”hyperon puzzle” and is presently the subject of active research.

Theoretical efforts to reconcile the presence of hyperons in the core of neutron stars with the observed masses of $2M_\odot$ are constructed primarily on very limited two-body hyperon-nucleon scattering data [12]. The $\Lambda p$ and $\Sigma^- p$ elastic scattering channels have been suggested to provide ”the most stringent constraints for the available theoretical models” [13].

Until recently, data for $\Sigma^- p$ elastic scattering has been scarce compared to the $\Lambda p$ channel, with only four publications from the bubble chamber era of the 1960s and 1970s [14, 15, 16, 17]. These experiments accumulated a total of 587 events, with $\Sigma^-$ momenta less than $200$ MeV/c. Higher momentum data measured 30 more events but with a large uncertainty [18]. No real progress has been made in the elastic scattering of $\Sigma^-$ from the proton since the 1970s due to experimental difficulties in producing hyperon beams. This is because, unlike in neutron star conditions where hyperons are stable, in terrestrial conditions hyperons are unstable and hence difficult to use as beams in scattering experiments.

A recent $\Sigma^- p$ scattering experiment performed at the J-PARC Hadron Experimental Facility [19] substantially improved the world data sample for the process with a total of 4500 elastic scattering events detected in the momentum range $470$ to $850$ MeV/c. The experiment used a secondary $\Sigma^-$ beam in a liquid deuterium target that was produced via the reaction $\pi^- p \to K^+ \Sigma^-$.

The success of the $\Sigma^- p$ scattering experiment is a promising milestone in strangeness physics, motivating the gathering of more data from different production methods. To this end, a feasibility study is presented where the incident $\Sigma^-$ beam is produced through photoproduction off a deuterium target via the process $\gamma n \to K^+ \Sigma^-$. The beam $\Sigma^-$ can then interact with a proton inside the target. The hyperon production and scattering events are simulated using Monte Carlo techniques.

This experimental method was first attempted with a photon beam in a $\Lambda p$ scattering experiment using the CLAS detector [20, 21], at the Thomas Jefferson National Accelerator Facility (JLab). The experiment used a hydrogen target and successfully increased the world data sample for this process by "well over an order of magnitude" [20]. However, the $\Sigma^-$ hyperon is generally a difficult beam to produce. The decay parameter for $\Sigma^-$ particles is $c\tau \sim 4.43$ cm, where $\tau$ is the lifetime and $c$ the speed of light, is even smaller than that of $\Lambda$ ($c\tau = 7.89$cm) [22]. Therefore, it is essential to examine the feasibility of this reaction and its potential to improve on the present data.

The present paper aims to study the feasibility of the $\Sigma^- p$ elastic scattering within the CLAS detector by simulating the reaction and detector response. Specifically, the feasibility of a reaction constitutes its acceptance within the detector, and the yield, i.e. expected number of scattering events detected, both of which will be measured in the simulation. A large number of detected events is a good indication that this could be a promising reaction for further analysis. Coupled with a good acceptance, the reaction could make a good candidate to be reproduced in the JLab facility with the CLAS detector.

In the following sections, an outline of the simulation is described, the method of calculating the energy of the beam is presented, as well as that of the luminosity, yield and cross sections. This is followed by a discussion of the results and a conclusion.

# 2 Methods

In this work, the reaction $\gamma n \to K + \Sigma^-$ was chosen as the method of producing a secondary $\Sigma^-$ beam to study the $\Sigma^- p$ elastic scattering. The reaction proceeds as follows:

$$\gamma n \to K^+ \Sigma^-; \quad \Sigma^- p \to \Sigma^- p; \qquad \Sigma^- \to n\pi^-$$

which is further illustrated in Figure 2. A 40 cm long cylindrical cell containing liquid deuterium is used to produce a hyperon beam and serve as a secondary target. The target setup is ideal for this analysis for two reasons. Firstly, deuterium makes a good source of quasi-free neutrons: as deuterium is bound by only $\sim 2$ MeV, an incident beam with energies of several hundred MeV can readily break it apart. This means that the target from the production vertex behaves much like a free, stationary neutron in the lab frame [23]. Secondly, the length of the target cell provides a sufficient number of potential secondary scattering targets for the rescattering process at vertex 2 (see Figure 2).

The incident photon beam is created from an electron bremsstrahlung process: the JLab accelerator produces an electron beam with energies of up to 6 GeV in CLAS which then interacts with the electromagnetic field of a radiator, i.e a gold foil [20]. The incoming electron with energy $E_0$, is accelerated by the field and emerges with lower energy $E_e$, emitting a photon of energy $E_\gamma$ by transferring a small amount of momentum $q$ to the nucleus [24]. The reaction obeys the energy conservation relation:

$$E_\gamma = E_0 - E_e \tag{1}$$

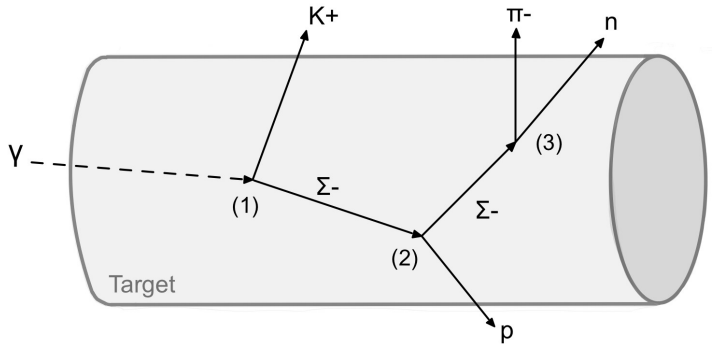


Figure 2: Schematic view of the reaction inside the deuterium target. On an event-by-event basis, $\Sigma^-$ is photoproduced at vertex (1), then propagates through the target until it scatters with a proton at rest at vertex (2) before it decays with nearly a 100% branching ratio to $n\pi^-$ at vertex (3).

This process is treated in the relativistic limit where bremsstrahlung is the dominant mode of energy loss for electrons, and the nuclear recoil energy is neglected [24].

The bremsstrahlung photon beam is then impinged on a deuterium target to produce the reaction in Figure 2. From an experimental standpoint, this reaction requires the detection of a $K^+$ and a $\pi^-$, as well as the scattered $\Sigma^-$ and scattered proton. With a detector covering a solid angle of $4\pi$ all the final-state particles can be observed [20], for which the CLAS detector in the Jlab facility is well-suited.

The Monte Carlo (MC) technique [25] was used to simulate this reaction. This technique utilises random sampling from probability distributions to model physical process described by these probabilities. For example, the scattering events are generated at random according to a phase-space distribution. Moreover, the photon energies are sampled from a distribution $\propto 1/x$, and decay path from a probability distribution $\propto e^x$, as will be shown in sections 2.1 and 2.3, respectively. The number of events $N$ generated then determines the precision as $\frac{1}{\sqrt{N}}$.

Root, a data analysis framework provided by CERN [26], was used for histogramming and graphing to view and analyse the MC data. The full code, written in C++, is found in Ref [32].

The simulation starts by generating the events which describe the interaction. This requires defining the four-momentum vectors of the initial-state particles [24], defined as

$$P = (Px, Py, Pz, E), \tag{2}$$

the masses of the final-state particles, and the energy of the centre of momentum. This was done for the three vertices of the reaction defined in Figure 2. The primary interaction target, a quasi-free neutron in a deuterium target, then interacts with a Bremsstrahlung photon beam.

The bremsstrahlung beam is not monoenergetic, and the events are generated within a specific range of energies using a random number generator. The following section describes the analysis used to calculate the minimum photon beam energy required to produce the $\Sigma^-$ beam.

## 2.1 Threshold Energy

In the laboratory reference frame,

$$P^{LAB} = P_\gamma + P_n \tag{3}$$

Since the target is static, $m_\gamma = 0$, $P_{z,\gamma} = E_\gamma$, and $E_n = m_n$. From Eq.2, The initial state four-momentum vector and its square, $s^{LAB}$, are given by [24, 27]

$$P^{LAB} = P_\gamma + P_n = (0, 0, E_\gamma, E_\gamma + m_n)$$
$$s^{LAB} = (P_\gamma + P_n)^2 = m_n^2 + 2E_\gamma m_n$$

Similarly for the centre of momentum (CM) frame, the final state four-momentum vector and its square, $s^{CM}$, are given by

$$P^{CM} = P_K + P_\Sigma = (0, 0, 0, m_K + m_\Sigma)$$
$$s^{CM} = (P_K + P_\Sigma)^2 = (m_K + m_\Sigma)^2$$

Using the fact that $s$ is Lorentz-invariant [20], $s^{LAB} = s^{CM}$, so

$$E_\gamma = \frac{(m_K + m_\Sigma)^2 - m_n^2}{2m_n^2} \tag{4}$$

From reported mass values in [22], the threshold value for the energy of the photon beam is $E_{\gamma,threshold} = 1.0521$ GeV [1]. The beam energy was then sampled according to the $1/E_\gamma$ photon flux distribution, where the tagged photon energy is between $1.05$ and $2.3$ GeV.

## 2.2 Yield, Luminosity and Cross Sections

The photon beam then interacts with the target, and the simulation randomly generates $K^+$ and $\Sigma^-$ particles uniformly throughout the target. The luminosity of the photon beam, defined by

$$\mathscr{L}_\gamma = \frac{N_A \times \rho_T \times l_T}{M} N_\gamma \tag{5}$$

is used to calculate the $\Sigma^-$ beam flux from the relationship

$$\sigma = \frac{N_\Sigma}{\mathscr{L}_\gamma} \tag{6}$$

where $\sigma$ is total cross section of $K^+\Sigma^-$, $N_A$ is Avogadro's number, $N_\gamma$ is the photon beam flux, $N_\Sigma$ is the $\Sigma^-$ beam flux, and $\rho_T$, $l_T$, $M$ are the mass density, length, and molar mass of the target, respectively.

Determining the number of $\Sigma^-$ particles produced thus requires knowledge of the $K^+\Sigma^-$ cross section. The $\gamma n \to K^+\Sigma^-$ reaction was studied in [28] and the theoretical results are used to estimate the total cross section in the simulation to be $1.5 \mu b$.

[1] For this calculation the natural system of units where c = 1 is used

After extracting the number of $\Sigma^-$ particles from Equation 5, the luminosity of the $\Sigma^-$ beam, $\mathscr{L}_\Sigma$, is calculated in a similar manner to Equation 4, where $N_\gamma$ is replaced by $N_\Sigma$, and the length of the target, $l_T$, is replaced by the average path-length of the $\Sigma^-$ particles as described in Section 2.3. Finally, the number of rescattered $\Sigma^-$ particles produced is given by

$$\sigma_{\Sigma^- p \to \Sigma^- p} = \frac{N_{\Sigma'}}{\mathscr{L}_\Sigma} \tag{7}$$

where $N_{\Sigma'}$ indicates the number of rescattered $\Sigma^-$ particles. The theoretical predictions and experimental measurements of the $\Sigma^- p$ elastic scattering cross sections are shown in Figure 3 [29]. Using the available measurements, $\sigma_{\Sigma^- p \to \Sigma^- p}$ is estimated to be $30$ mb.

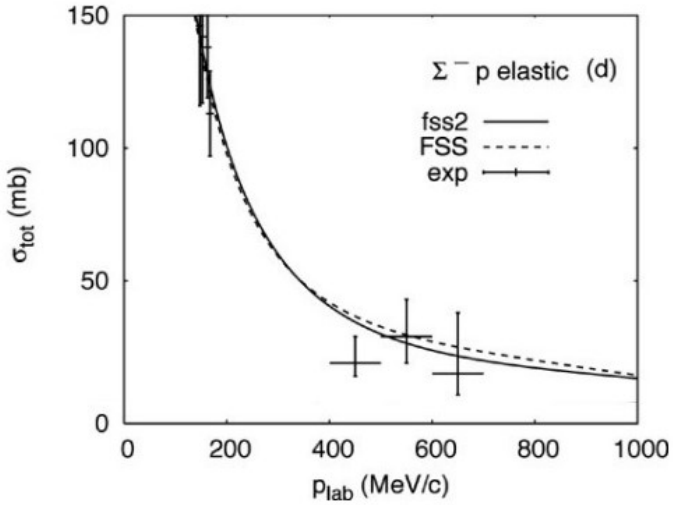


Figure 3: $\Sigma^- p$ elastic scattering total cross sections from theoretical models and experimental data [29].

Equation 6 is used to calculate the number of rescattered $\Sigma^-$ particles produced, but the number of rescattered $\Sigma^-$ particles measured has to take into account the simulated detector acceptance, $A$, so that

$$N_{\Sigma',detected} = \sigma_{\Sigma^- p \to \Sigma^- p} \times \mathscr{L}_\Sigma \times A_{\Sigma'} \tag{8}$$

The acceptance of rescattered $\Sigma^-$ particles represents the fraction of rescattered events visible to the detector due to its geometry. The 'blind' regions of the CLAS detector imposed angular and momentum constrains on all the final-state particles, i.e. $K^+$, rescattered $\Sigma^-$, rescattered proton, and $\pi^-$ decay product. Only the events generated with angles in the range $10 - 160^\circ$ and momenta $> 200$ GeV are accepted. The ratio of constrained events and generated events represents the acceptance of the detector.

An important result of the simulation is the number of events from this reaction accepted by the detector, compared to the total number of events generated:

$$A = \frac{N_{accepted}}{N_{generated}} \tag{9}$$

In other words, if we generate X number of the desired $\Sigma^- p$ scattering events, how many of these will our detector be able to detect?

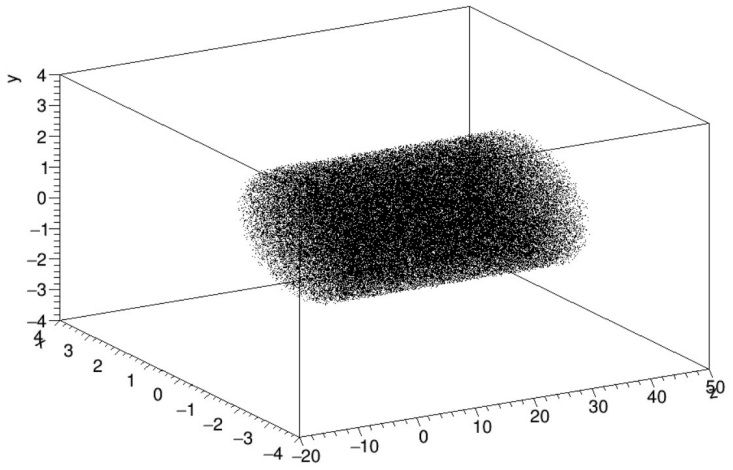


Figure 4: Monte-Carlo-generated $\Sigma^- p$ vertices throughout the cylindrical target.

## 2.3 $\Sigma^-$ Decay Path Length

The simulation randomly generates $\Sigma^-$ particles uniformly throughout the target, as visualised in Figure 4. The $\Sigma^-$ particle is then propagated through the target and its path length is derived from the production vertex and the geometry of the target cell. The longitudinal path and exit $z$ coordinate are calculated as (see Appendix)

$$\ell_l = \frac{\ell}{\tan(\theta)},$$
$$z_{exist} = \ell_l + z_0$$

Using $z_{exit}$, all possible exit mechanisms can be accounted for in order to simulate propagation in a realistic manner. For $z_{exit}$ between $0$ and $l_T$ where $l_T$ was defined as the length of the target, the path is given by

$$\text{Path} = \frac{\ell}{\sin(\theta)} \tag{10}$$

For $z_{exit}$ outside the target cell length, i.e. $z_{exit} < 0$ or $z_{exit} > l_T$, then the particle could exit through the end-caps. This is especially the case if it was produced at a small angle and/or close to either end of the target. In this case the path length is given by

$$\text{Path} = \begin{cases} \dfrac{l_T - z_0}{\cos(\theta)}, & \theta < 90^\circ \\ \dfrac{z_v}{\cos(\theta)}, & \theta > 90^\circ \end{cases} \tag{11}$$

where $z_0$ is the $z$ vertex coordinate. The $\Sigma$ beam decay parameter, $c\tau = 4.43$cm, is much smaller than the length of the target, $40$cm. Therefore, $\Sigma^-$ could decay before it exits the cylinder or interacts with a proton. In this case, the path length is given by

$$\text{Path} = \beta\gamma c\tau \tag{12}$$

with velocity $\beta = v/c$, and Lorentz boost $\gamma$. The final path length is weighted by the probability of particle decay given by

$$P(d) = exp\left(\frac{-d}{\beta\gamma c\tau}\right) \tag{13}$$

where $d$ is the distance the particle travels without decaying.

# 3 Results and Discussion

The simulations results that follow are based on a 100 days of beamtime with a total of $1.0368 \times 10^{14}$ photons impinging on a 40 cm long liquid deuterium target of radius 2 cm and density $0.1630\ g\ cm^{-3}$. The photon beam energies range from $1.05$ to $2.3$ GeV, with a total flux of $1.0368 \times 10^{14}$ bremsstrahlung photons over the 100 days. These photons produce $\Sigma^-$ particles inside the target by means of photoproduction.

Figure 5 shows the kinematics of the $\Sigma^-$ beam produced from photoproduction, some of which will now go-on to scatter further with static protons as discussed in the previous section. The angular dependence illustrates the properties of the $\Sigma^-$ beam.

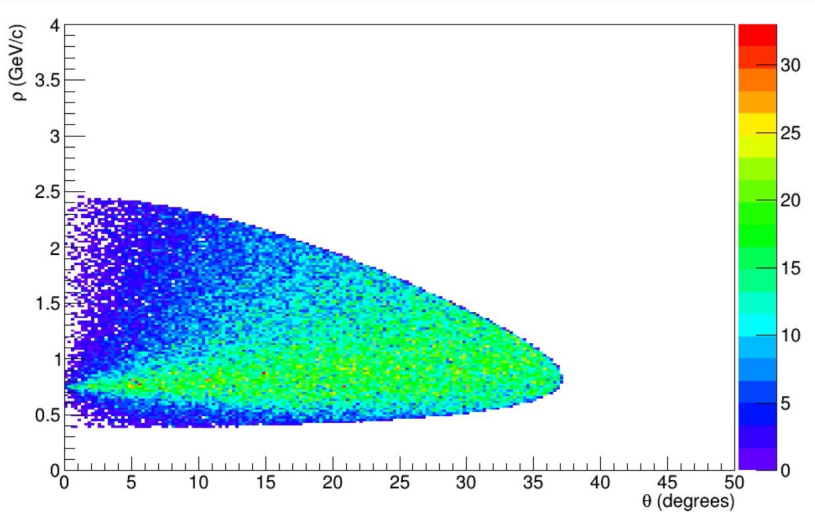


Figure 5: The angular dependance of the $\Sigma^-$ beam from simulation. The colour bar at the side represents a color scale that shows the number of events in each bin.

Looking at the figure, it is clear that $\Sigma^-$ particles that are produced with relatively small angles relative to the photon beam axis tend to have higher momenta. This is to be expected on the basis of basic kinematics. However, in this particular experimental arrangement it also implies that higher momenta particles are also more likely to scatter since they will tend to propagate from their formation vertex into a greater depth of the target cell.

It can also be seen that the momentum range of the produced $\Sigma^-$ particles is $0.5$ to $2.5$ GeV/c. This upper limit of momentum is higher than that which has been produced before. Previously the highest recorded scattering experiment momenta are those described in reference [19] which extended to only 0.85 GeV/c. Such an experiment

could therefore extend the $\Sigma^-$ scattering dataset to higher momenta, which would help constrain hyperon-nucleon scattering models, as the uncertainties at higher scattering momenta are particularly marked and also most relevant to the conditions near the centre of a neutron star [30]. For completeness, the angular dependence for each final-state particle after angular and momentm cuts were applied are shown in Figure 6.

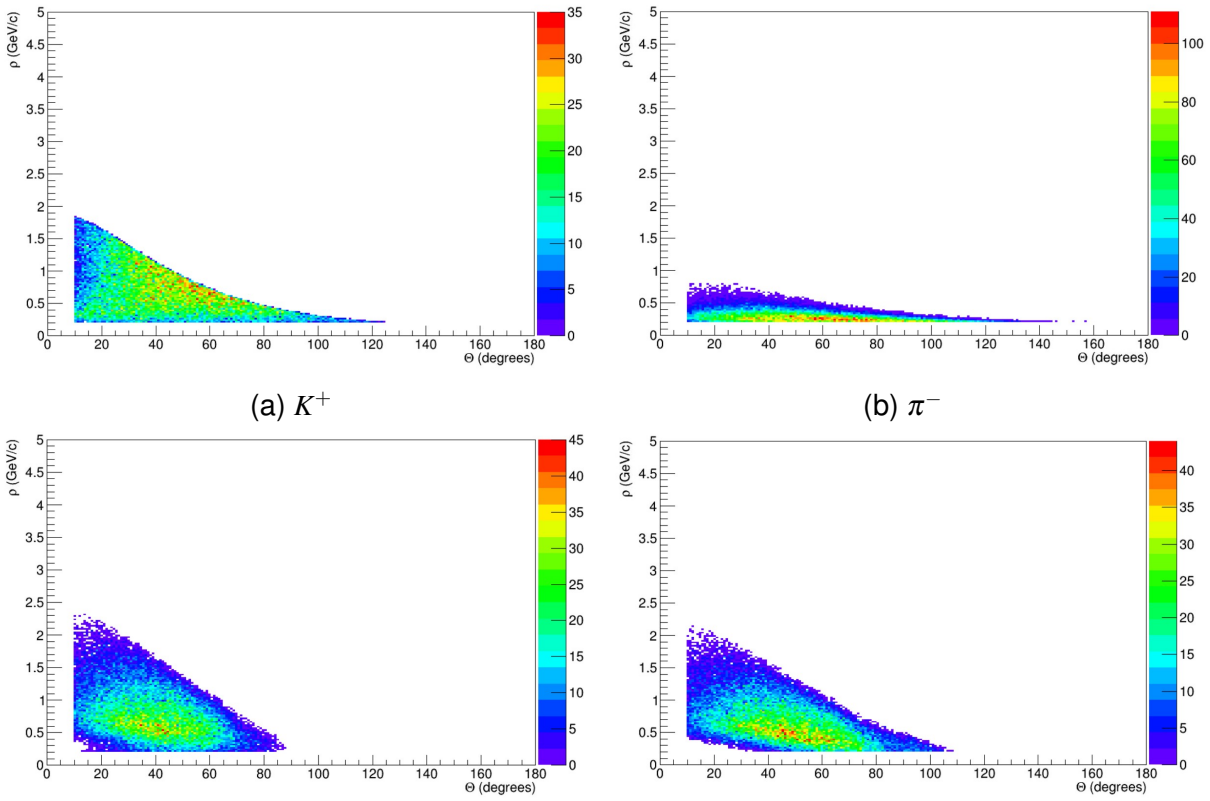


(a) $K^+$ (b) $\pi^-$

(c) Rescattered $\Sigma^-$ (d) Rescattered $p$

Figure 6: The constrained kinematics of the final-state particles. The colour bar represents a color scale that shows the number of events in each bin

The $\Sigma^-$ beam produced as described is now further propagated from the formation vertices and on through the target. Figure 7a shows the longitudinal path length of $\Sigma^-$ before it either rescatters or exits the target. As anticipated, the $\Sigma^-$ particles produced at relatively small angles with respect to the photon beam axis tend to propagate larger distances through the target. Figure 7b shows the grand path length which takes into account particle decay. It can be seen that some of the $\Sigma^-$ decay relatively quickly (distance $<$ 5cm) while others cover a larger distance before decaying.

Figure 8a and Figure 8b show the $z$ and $x-y$ coordinates of the decay vertices, respectively. The vertical lines in Figure 8b represent the boundaries of the deuterium target based on its width (4 cm). It is clear that some of the particles pass through the cylindrical wall of the target and decay outside of it, while the majority decay inside the target, as shown in Figure 7b.

The photoproduced $\Sigma^-$ particles can either decay without scattering, exit the target without scattering, or scatter off a proton. All these cases were taken into account for

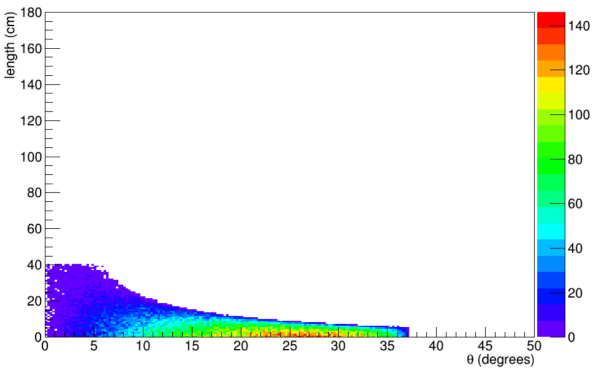


(a) $\theta$ vs the longitudinal path length of $\Sigma^-$

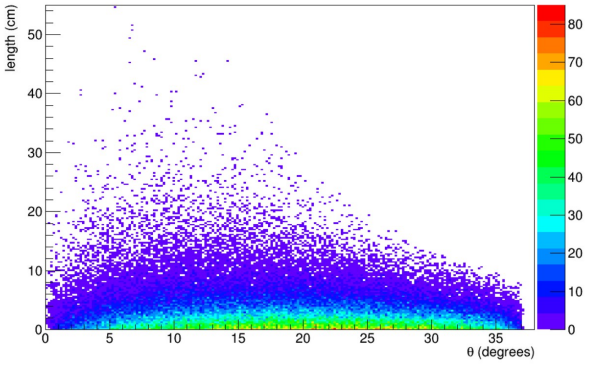


(b) $\theta$ vs the decay path length of $\Sigma^-$

Figure 7: $\theta$ vs the path length of $\Sigma^-$ before scatterigt (a), or decaying (b). The colour bar represents a color scale that shows the number of events in each bin.

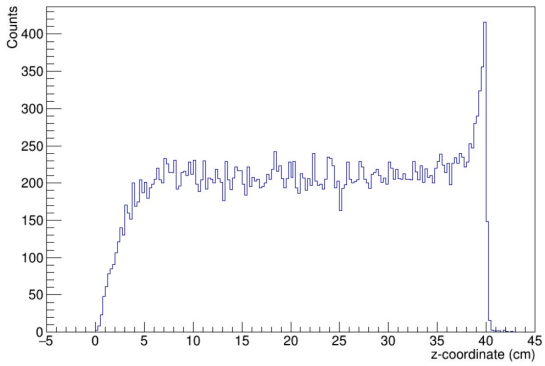


(a) $z$-coordinates

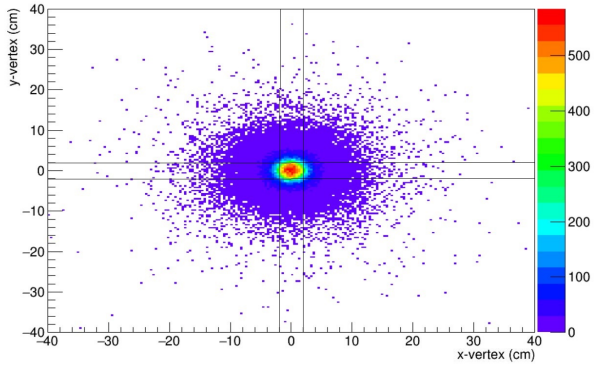


(b) $x-y$ vertex

Figure 8: Decay coordinates distribution for the $\Sigma^-$ decay vertex. The lines in (b) represent the cylinder boundaries, the colour bar represents a color scale that shows the number of events in each bin.

the simulation of the $\Sigma^-$ beam path length. The mean value of the path length is found to be 3.2 cm. This is relatively short as compared to the length of the target cell (40 cm), however it is the angular distribution of the path length which has the greatest impact on the number of scattering events.

A $\Sigma^-$ particle which was produced, say, at the entrance of the target and on the target axis, would have roughly 40 cm to travel before it leaves the target (assuming it doesn't decay). However, if the angle at which it was produced was close to $90^\circ$, then the particle only has about 2 cm to travel before it exits the target, as seen in Figure 8b. Hence, the angular distribution of the $\Sigma^-$ particles directly determines their individual contributions to the luminosity based on their path length. This, in turn, affects the yield for the scattering events.

The total photon flux, was $1.0368 \times 10^{14}$ over the 100 days of beam time, which was used to calculate the photon beam luminosity, as given by Equation (5). The photon

beam luminosity is then

$$\mathscr{L}_\gamma = \frac{6.02 \times 10^{23} \times 0.1630 \times 40 \times 1.0368 \times 10^{14}}{2.014}$$
$$= 2.02 \times 10^{38} cm^{-2} \text{ per 100 days}$$

or $1.40 \times 10^{33} cm^{-2}$ per second. In the simulation, the beam luminosity was calculated for each run and used to obtain the flux of the $\Sigma^-$ beam. The result was $3.03 \times 10^8$ over the 100 days. From this, and the mean decay path length (3.2 cm), the $\Sigma^-$ beam luminosity was found as an intermediate step to extracting the yield of the scattered $\Sigma^-$.

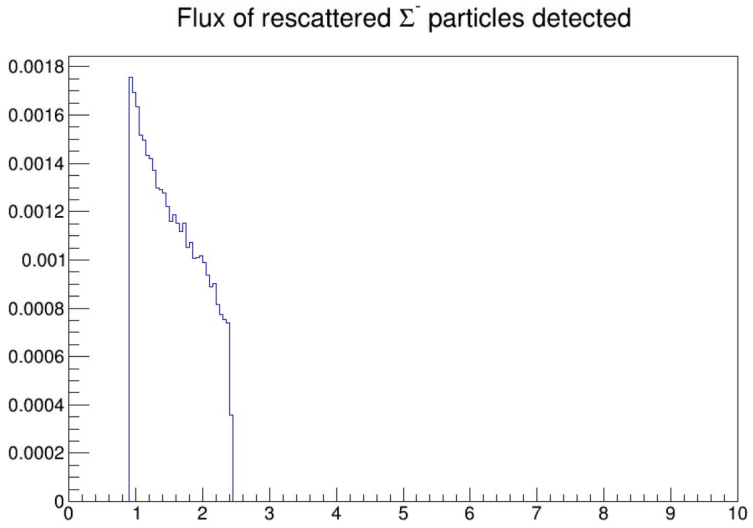


Figure 9: Number of $\Sigma^- p$ elastic scattering events measured per second.

As discussed in the introduction, the main goals of this study were to find out the number of $\Sigma^- p$ scattering events, both produced and detected, and the acceptance. Based on the simulations performed, the total number of $\Sigma^- p$ scattering events was found to be $1.43 \times 10^6$ ($\pm 0.08\%$) over 100 days, and the total number of $\Sigma^- p$ scattering events detected (Figure 9) was found to be $306,790$ ($\pm 0.2\%$) over the 100 days. The acceptance for this reaction is thus (Equation 9)

$$A = \frac{N_{accepted}}{N_{generated}} = 21\% \pm 0.25\%$$

The measured yield is much higher than the experimental data from [14, 15, 16, 17] combined. This matches the results in [20], where use of the photoproduction of $\Lambda$ method was found to significantly increase the number of $\Lambda p$ scattering events. Approximately 20% of the total number of $\Sigma^- p$ elastic scatterings observed were measured, hence the CLAS detector would be able to detect the sacttering events from this reaction.

The $\Sigma^- p$ elastic scattering has not been measured before from the reaction $\gamma n \rightarrow K^+ \Sigma^-$, the results shown here suggest that it is a promising reaction for further analysis.

The next step from this would be to perform a full-scale simulation using Geant4 software [31] or similar. Geant4 was originally developed by CERN as a particle transport simulation software emplying Carlo methods, which takes into account the dynamics of the reaction, and the details of the CLAS detector geometry. Such an investigation would consider the systematic uncertainties from the experimental set-up, rather than just statistical (simulation) uncertanties, as was done in this work.

# 4 Conclusions

A feasibility study is presented where the incident $\Sigma^-$ beam is produced through photoproduction off a deuterium target via the process $\gamma n \to K^+\Sigma^-$. The beam $\Sigma^-$ can then interact with a proton inside the target and the $\Sigma^- p$ elastic scattering events are identified by measuring four-momentum vectors of the initial and final state particles. The $\gamma n \to K^+\Sigma^-$ total cross section was estimated in the simulation to be $1.5\mu b$, and the $\Sigma^- p \to \Sigma^- p$ total cross section $30mc$.

The Monte Carlo (MC) technique was used to simulate this reaction. The scattering events were generated at random according to a phase-space distribution, the photon energies were sampled from a distribution $\propto 1/E_\gamma$, and finally the decay path was sampled from a probability distribution $\propto e^x$. The number of events $N$ generated then determines the precision as $\frac{1}{\sqrt{N}}$.

The threshold energy of the photon beam was estimated to be 1.05 GeV. The photon beam produced $\Sigma^-$ particles inside the target by means of photoproduction. There was a total of $3.03 \times 10^6$ $\Sigma^-$ beam particles running in the target per day. The total number of $\Sigma^- p$ scattering events produced was $1.43 \times 10^6$ ($\pm 0.08\%$), over the 100 days of beamtime, of which $21\% \pm 0.25\%$ were measured, giveing a yield of $306,790$ ($\pm 0.2\%$) over the 100 days for the $\Sigma^- p$ elastic scattering.

Therefore, this study supports the feasibility the $\Sigma^- p$ elastic scattering expeiment in JLab. A high elastic scattering yield was achieved for the hyperon beam in the momentum range 0.5 ro 2.5 GeV/c which is of importance to neutron star physics to help constrain the neutron star EOS. While these results are promising, it should be borne in mind that the investigation here used a simplified simulation method which did not include the dynamics of the reaction. Further studies will be required as a next step in order to form the basis of a robust experimental proposal.

# A Path length Calculation

Let the cylindrical target cell be aligned with the z-axis and the centre located at $(0,0,l_T/2)$ where $l_T = 40$ cm. Vertex coordinates $x_0, y_0$ are generated uniformly and randomly on a disc with the same radius as the cylinder (2 cm). The azimuthal angle $\phi_V$ of the vertex position measured from the positive $x$ axis is obtained from uniformly distributed random numbers between $0, 2\pi$. The distance from the center of the target to the vertex position, $r_0$, is sampled as

$$r_V = \sqrt{Rnd} \times r$$

where Rnd represents a random number in $[0,1]$, and $r$ is the radius of the cylinder. The distance along the $z$-axis is sampled uniformly from $0$ to $40$ cm. The vertex position is thus given by

$$\begin{aligned} x_0 &= r_0 \times \cos(\phi_V) \\ y_0 &= r_0 \times \sin(\phi_V) \\ z_0 &= z_0 \end{aligned}$$

For a given trajectory with angle $\phi_p$, the expression of the path length $\ell$ can be derived by simple geometry. The figure below shows an example trajectory in $xy$ plane, ie looking into the cylinder.

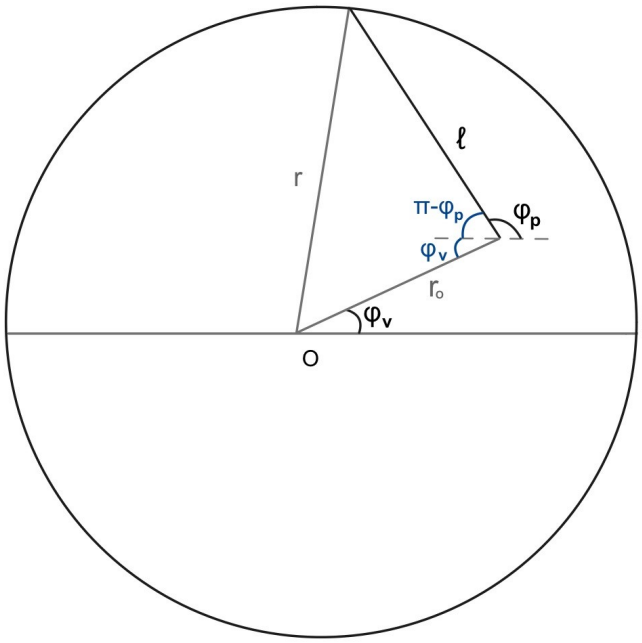


Figure 10: Example path projection on $xy$ plane

From the cosine rule,

$$\begin{aligned} r^2 &= r_0^2 + \ell^2 - 2r_0\ell\cos(\pi - \phi_p + \phi_v) \\ &= r_0^2 + \ell^2 - 2r_0\ell\cos(\pi - (\phi_p - \phi_v)) \end{aligned}$$

using $\cos(\pi - x) = -cos(x)$,

$$r^2 = r_0^2 + \ell^2 + 2r_0\ell\cos(\phi_p - \phi_v)$$

rearranging into the form $ax^2 + bx + c = 0$,

$$\ell^2 + [2r_0\cos(\phi_p - \phi_v)]\ell + r_0^2 - r^2 = 0$$

and solving using the quadratic equation

$$\ell = \frac{-[2r_0\cos(\phi_p - \phi_v)] \pm \sqrt{[2r_0\cos(\phi_p - \phi_v)]^2 - 4(r_0^2 - r^2)}}{2},$$

finally gives the path in $xy$ plane

$$\ell = -r_0\cos(\phi_p - \phi_v) \pm \sqrt{r_0^2\cos^2(\phi_p - \phi_v) + r^2 - r_0^2}$$

The longitudinal path is then given by

$$\ell_l = \frac{\ell}{\tan(\theta)} \tag{14}$$

and the $z$ coordinate of the exit position is

$$z_{exist} = \ell_l + z_0 \tag{15}$$

# References


[1] G. D. ROCHESTER. and C. C. BUTLER, *Evidence for the Existence of New Unstable Elementary Particles*, Nature **160**, 855 (1947).

[2] M. Danysz and J. Pniewski, *Delayed Disintegration of a Heavy Nuclear Fragment: I*, The London, Edinburgh, and Dublin Philosophical Magazine and Journal of Science **44**, 348 (1953).

[3] A. Feliciello and T. Nagae, *Experimental Review of Hypernuclear Physics: Recent Achievements and Future Perspectives*, Reports on Progress in Physics **78**, (2015).

[4] V. A. Ambartsumyan and G. S. Saakyan, *The Degenerate Superdense of Elementary Particles*, Soviet Astronomy **4**, 187 (1960).

[5] I. Vidana, A. Polls, A. Ramos, O. Elgaroey, L. Engvik, and M. Hjorth-Jensen, *Properties of $\beta$-Stable Neutron Star Matter with Hyperons*, ArXiv:nucl-Th/9912016 (1999).

[6] I. Bombaci, *Strangeness in Neutron Stars*, Nuclear Physics A **754**, 335 (2005).

[7] J. M. Lattimer and M. Prakash, *Neutron Star Structure and the Equation of State*, The Astrophysical Journal **550**, 426 (2001).

[8] K. Aoki, H. Fujioka, T. Gogami, Y. Hidaka, E. Hiyama, R. Honda, A. Hosaka, Y. Ichikawa, M. Ieiri, M. Isaka, N. Ishii, T. Ishikawa, Y. Komatsu, T. Komatsubara, G. Lim, K. Miwa, Y. Morino, T. Nagae, S. Nagao, and S. N. Nakamura, *Extension of the J-PARC Hadron Experimental Facility: Third White Paper*, ArXiv:2110.04462 [Hep-Ex, Physics:nucl-Ex, Physics:nucl-Th, Physics:physics] (2021).

[9] I. Vidaña, Hyperons: *The Strange Ingredients of the Nuclear Equation of State*, Proceedings of the Royal Society A: Mathematical, Physical and Engineering Sciences **474**, 20180145 (2018).

[10] P. Demorest, T. Pennucci, S. Ransom, M. Roberts, and J. Hessels, Shapiro Delay *Measurement of a Two Solar Mass Neutron Star*, Nature **467**, 1081 (2010).

[11] J. Antoniadis, P. C. C. Freire, N. Wex, T. M. Tauris, R. S. Lynch, M. H. van Kerkwijk, M. Kramer, C. Bassa, V. S. Dhillon, T. Driebe, J. W. T. Hessels, V. M. Kaspi, V. I. Kondratiev, N. Langer, T. R. Marsh, M. A. McLaughlin, T. T. Pennucci, S. M. Ransom, I. H. Stairs, and J. van Leeuwen, *A Massive Pulsar in a Compact Relativistic Binary*, Science **340**, 448 (2013).

[12] K. Miwa, J. K. Ahn, Y. Akazawa, T. Aramaki, S. Ashikaga, S. Callier, N. Chiga, S. W. Choi, H. Ekawa, P. Evtoukhovitch, N. Fujioka, M. Fujita, T. Gogami, T. Harada, S. Hasegawa, S. H. Hayakawa, R. Honda, S. Hoshino, K. Hosomi, and M. Ichikawa, *Study of $\Sigma N$ Interaction from the $\Sigma - P$ Scattering Experiment at J-PARC*, Journal of Physics: Conference Series 1643, (2020).

[13] L. Tolos and L. Fabbietti, Strangeness in Nuclei and Neutron Stars, *Progress in Particle and Nuclear Physics*, **112**, 103770 (2020).

[14] H. G. Dosch, R. Engelmann, H. Filthuth, V. Hepp, E. Kluge, and A. Minguzzi-Ranzi, *Low-Momentum Interactions of $\Sigma$ Hyperons with Protons*, Physics Letters **14**, 162 (1965).

[15] H. G. Dosch, R. Engelmann, H. Filthuth, V. Hepp, and E. Kluge, *Elastic $\Sigma - P$ Scattering at Low Momenta*, Physics Letters **21**, 236 (1966).

[16] H. A. Rubin and R. A. Burnstein, *Low-Energy ($\Sigma^+, P$) and ($\Sigma^-, P$) Elastic Scattering*, Physical Review **159**, 1149 (1967).

[17] F. Eisele, H. Filthuth, W. Föhlisch, V. Hepp, and G. Zech, *Elastic $\Sigma \pm P$ Scattering at Low Energies*, Physics Letters B **37**, 204 (1971).

[18] Y. Kondo, J. K. Ahn, H. Akikawa, J. Arvieux, B. Bassalleck, M. S. Chung, H. En'yo, T. Fukuda, H. Funahashi, S. V. Golovkin, A. M. Gorin, Y. Goto, M. Hanabata, T. Hayakawa, A. Ichikawa, M. Ieiri, K. Imai, M. Ishino, H. Kanda, and Y. D. Kim, *$\Sigma - P$ Elastic-Scattering in the Region of 400*, Nuclear Physics A **676**, 371 (2000).

[19] K. Miwa, J. K. Ahn, Y. Akazawa, T. Aramaki, S. Ashikaga, S. Callier, N. Chiga, S. W. Choi, H. Ekawa, P. Evtoukhovitch, N. Fujioka, M. Fujita, T. Gogami, T. Harada, S. Hasegawa, S. H. Hayakawa, R. Honda, S. Hoshino, K. Hosomi, and M. Ichikawa, *Measurement of the Differential Cross Sections of the $\Sigma - P$ Elastic Scattering in Momentum Range 470 to 850 MeV/C*, Physical Review C 104, (2021).

[20] J. Price, *$\Lambda p$ Elastic Scattering in the CLAS Detector*, 2019.

[21] B. A. Mecking, G. Adams, S. Ahmad, E. Anciant, M. Anghinolfi, B. Asavapibhop, G. Asryan, G. Audit, T. Auger, H. Avakian, J. P. Ball, F. J. Barbosa, S. Barrow, M. Battaglieri, K. Beard, B. L. Berman, N. Bianchi, S. Boiarinov, P. Bonneau, and W. J. Briscoe, *The CEBAF Large Acceptance Spectrometer (CLAS), Nuclear Instruments and Methods in Physics Research Section A: Accelerators, Spectrometers, Detectors and Associated Equipment*, **503**, 513 (2003).

[22] Particle Data Group - *2020 Review*, https://pdg.lbl.gov/.

[23] K. H. HICKS, K. ARDASHEV, M. BLECHER, A. CARACAPPA, A. CICHOCKI, C. COMMEAUX, A. D'ANGELO, J.-P. . DIDILEZ, R. DEININGER, S. HOBLIT, M. KHANDAKER, O. KISTNER, A. KUCZEWSKI, F. LINCOLN, R. LINDGREN, A. LEHMANN, M. LOWRY, M. LUCAS, H. MEYER, and L. MICELI, *NEUTRAL PION PRODUCTION from DEUTERIUM at the LEGS FACILITY*, Electromagnetic Interactions in Nuclear and Hadron Physics (2002).

[24] M. A. Segura, J. Salamanca, and E. Munevar, *Monte Carlo Threshold Energy Estimation for a + B $\rightarrow$ c + D Processes: An Educational Resource in Experimental High Energy Physics Research*, Revista Brasileira de Ensino de Física 39, (2016).

[25] Monte Carlo Simulation - *an Overview ScienceDirect Topics*, https://www.sciencedirect.com/topics/economics-econometrics-and-finance/monte-carlo-simulation.

[26] R. Brun and F. Rademakers, *ROOT — an Object Oriented Data Analysis Framework*, Nuclear Instruments and Methods in Physics Research Section A: Accelerators, Spectrometers, Detectors and Associated Equipment **389**, 81 (1997).

[27] D. J. Griffiths, *Introduction to Elementary Particles* (Wiley-Vch, Weinheim, 2011).

[28] I. Niculescu, *Photoproduction on the Neutron: Results from CLAS*, 2019.

[29] Y. Fujiwara, Y. Suzuki, and C. Nakamoto, Baryon–Baryon Interactions in the SU6 Quark Model and Their Applications to Light Nuclear Systems, *Progress in Particle and Nuclear Physics*, **58**, 439 (2007).

[30] J. Rowley, N. Compton, C. Djalali, K. Hicks, J. Price, N. Zachariou, K. P. Adhikari, et al. Improved Lambda P Elastic Scattering Cross Sections between 0.9 and 2.0 GeV/c as a Main Ingredient of the Neutron Star Equation of State, Physical Review Letters 127, (2021).

[31] S. Agostinelli, J. Allison, K. Amako, J. Apostolakis, H. Araujo, P. Arce, M. Asai, D. Axen, S. Banerjee, G. Barrand, F. Behner, L. Bellagamba, J. Boudreau, L. Broglia, A. Brunengo, H. Burkhardt, S. Chauvie, J. Chuma, R. Chytracek, and G. Cooperman, *Geant4-a Simulation Toolkit, Nuclear Instruments and Methods in Physics Research Section A: Accelerators, Spectrometers, Detectors and Associated Equipment* **506**, 250 (2003).

[32] A. Ghaleb, Sigma proton.c, (2022), GitHub repository, https://github.com/aya-gh19/Sigma_proton.c